Electrochimica Acta 365 (2021) 137088

Contents lists available at ScienceDirect

Electrochimica Acta

journal homepage: www.elsevier.com/locate/electacta

Synergistic effect of sulfur-rich copolymer/S_8 and carbon host porosity in Li-S batteries

Ayda Rafie, Arvinder Singh, Vibha Kalra*

Department of Chemical and Biological Engineering, Drexel University, Philadelphia, PA, 19104, USA

ARTICLE INFO

Article history:
Received 2 July 2020
Revised 16 August 2020
Accepted 7 September 2020
Available online 9 October 2020

Keywords:
Carbon nanofibers
Sulfur-rich copolymers
Lithium-sulfur batteries
Porosity
Polysulfide shuttle

ABSTRACT

In this work, we investigate the possible role of host material porosity in performance of Li-S batteries, when sulfur-rich copolymer is used as an active ingredient in the cathode. We synthesized a freestanding cathode material using electrospun carbon nanofibers (CNFs) and poly(sulfur-random-1,3-diisopropenylbenzene)/SDIB (with some residual unreacted sulfur) and used it without adding any binders or current collectors. To study the effect of porosity of CNFs, two different porous samples, microporous (miCNF) and mesoporous (meCNF), were designed. When miCNF was used as a host material, the capacity stabilized to 577 mAh/g within 50 cycles and remained stable up to 600 cycles with a small capacity decay rate of 0.046% per cycle along with an excellent coulombic efficiency of >98% throughout the 600 cycles. On the other hand, SDIB-meCNF cathodes delivered a stable capacity of ~600 mAh/g with negligible decay. However, the stability only lasted for 145 cycles. Despite the positive effect of C-S bond formed in SDIB active material, we hypothesize that the porosity of the cathode host still plays a significant role not only due to residual unreacted S_8 in the original cathode, but also due to additional loose soluble -S_n- chains that emerge from S-S bond breakage in C-S-S_n-S-C (SDIB) over the course of cycling. Moreover, using the effective capacity calculation, we compared the discharge capacity of our cathode to other works on sulfur rich copolymers at C/2 and C/5 rates. The effective capacity analysis clearly manifests the advantages of using current-collector and binder-free electrospun CNFs as a host matrix for SDIB.

1. Introduction

The capacity and energy density of Li-ion batteries has reached their theoretical limit [1]. Among the newer technologies, Li-S batteries are closer to commercialization [2]. The Li-S battery uses sulfur instead of heavy metals used in Li-ion batteries, which has a tremendous environmental impact [3]. The metal oxides used in Li-ion batteries are heavy and expensive, where sulfur is a byproduct in refineries which makes it cheap and abundant [4]. Li-S battery offers a theoretical gravimetric energy density of ~2500 Wh/kg, which is more than five times higher than Li-ion batteries [5]. Despite these advantages over Li-ion batteries, there are several challenges impeding the commercialization of Li-S batteries. These challenges include: (1) Insulating nature of sulfur and Li_2S (2) polysulfide shuttling phenomena (3) mechanical failure as a result of expansion due to the conversion of S_8 to Li_2S. Several strategies have been employed to solve the mentioned challenges in different ways. For example, different host materials can be designed to reduce the lithium polysulfide shuttle challenge [1,6]. Various host materials such as carbonaceous [7], metal oxides, sulfides and nitrides [8,9], polymers [10,11], and metal-organic frameworks [12] have been studied in the past. Electrolyte modification is another area of research where an additive, co-salt or co-solvent is added to the electrolyte to tune the Li^+ ion diffusion, viscosity, polysulfide dissolution rate or formation of a stable solid electrolyte interphase [13-15]. All the strategies mentioned above utilize pure elemental sulfur (S_8) as the active material. Covalent fixing of sulfur to unsaturated carbon- carbon or heteroatoms bonds has been recently considered as a promising approach to improve the electrochemical properties of sulfur cathodes. In this regard, several inorganic compounds, such as selenium and phosphorus sulfides, organosulfur compounds and sulfur-embedded polymers have been studied [16]. In 2013, a new class of sulfur-rich copolymer was synthesized by Pyun et al. [11]. A process termed “inverse vulcanization” reaction was used to react a monomer with sulfur at temperatures higher than its ring opening temperature.

In 2014, first study on sulfur-rich copolymer based Li-S batteries was published [17]. The general hypothesis was that the C-S bond formed as a result of sulfur diradical stabilization, can

* Corresponding author.
E-mail address: vk99@drexel.edu (V. Kalra).

https://doi.org/10.1016/j.electacta.2020.137088
0013-4686/

chemically bind the lithium polysulfides formed during cycling, which would significantly decrease the shuttling phenomena. In this work, 10 wt% 1,3-diisopropenylbenzene (DIB) was used, and the slurry of poly(sulfur-random-1,3-diisopropenylbenzene) (SDIB) copolymer (75%), carbon black and binder (25%) was coated onto carbon coated aluminum foil and was used as the cathode. The battery showed a high initial capacity of 1100 mAh/g at C/10 which was reduced to 823 mAh/g after 100 cycles [18]. Although the work demonstrated relatively low cycle life, it showed that the sulfur-rich polymers fabricated via inverse vulcanization reaction could be a potential candidate to stabilize sulfur in cathode side and reduce shuttling in Li-S battery. Inspired by this idea, a handful of studies were conducted using inverse vulcanization reaction to fabricate sulfur-rich copolymers focusing on the use of different monomers with various functionalities [17,19-22]. For example, sustainable cardinal based benzoxazine have been studied as a monomer for inverse vulcanization reactions, where a sustainable electrode material is synthesized and tested as a cathode in Li-S batteries [23,24]. However, to the best of our knowledge, none of the studies discuss the role of cathode host material in enhancing the polysulfide suppressing functionality of such chemically-bound active material. Moreover, all of these cathodes are powder-based resulting in a need for additional dead weight from binding agents, a separate heavy (3–5 mg/cm^2) current collector (Al foil), and extensive slurry processing to fabricate the cathode.

In this work, we aim to study the possible effect of host porosity when sulfur rich copolymers are used as active material. We have designed a freestanding, binder-free cathodes using the SDIB copolymer and carbon nanofiber (CNF) mats. To study the effect of porosity, we used electrospinning method to fabricate porous CNFs [25]. Two different samples were fabricated, miCNFs with high micropore volume and relatively small mesopore volume and meCNFs with similar microporosity, but significantly higher mesopore size and volume. Using electrospinning, we have eliminated the need for insulating binders used in conventional slurry processing. The binders can block the pores of the host material and result in a sluggish cathode morphology. Therefore, our electrospun porous CNFs can act as a model to truly investigate the effect of porosity without having changes in morphology of the cathode upon cycling. As a reference, we also made sulfur-based cathode material which lasts for less than a hundred cycles, whereas our SDIB cathode material showed a capacity loss for the first couple of cycles but then remained very stable up to 600 cycles. The result of our electrochemical experiment shows that miCNFs can help us achieve higher capacity retention. Even though as we confirm with TGA, the copolymer is not incorporated in the pores, but we believe that the existence of loose sulfur (i.e., unreacted) and C-S-S_n-S-C breakage, results in the gradual formation of lithium polysulfides, that can be trapped in micropores of the CNFs. Because the copolymer is not confined in the pores, the lithium polysulfide trapping mechanism is very similar to the effect of microporous interlayer as reported in the literature [26]. Our results also suggested that as we move towards a higher mesopore size and volume, the electrolyte accessibility increases, and higher capacity can be achieved. However, the higher capacity means higher polysulfide formation and need for entrapment. Moreover, the existence of the larger mesopores in meCNFs possibly leads to easier escape of the formed polysulfides, resulting in early capacity fade in batteries [25,27,28]. Our results show that optimization of the pore structure is necessary to maintain cycling stability, concluding that there are loose sulfur and polysulfides in our system. We believe that this loose sulfur is originated from unreacted sulfur in the initial material and additional loose sulfur formed during cycling. In addition to the host porosity study, the effective capacity calculation clearly confirms the advantage of our SDIB-CNF cathode compared to the reported values based on the powdered/slurry-based sulfur-rich copolymer cathodes in literature. In this regard, we adjusted the discharge capacity of the batteries based on the total weight of the cathode by considering the additional weight of the binders, conductive material, and heavy current collectors, that are used in other studies.

2. Experimental methods

2.1. Fabrication of CNFs and porous CNFs

Electrospinning technique was used to prepare CNF, miCNF and, meCNF samples as reported previously by our group [25]. Briefly, for CNF samples, 10 wt% polyacrylonitrile (PAN, average MW: 150,000, Sigma-Aldrich) was dissolved in N,N-dimethylformamide (DMF, Sigma Aldrich) overnight. For miCNF and meCNF samples, PAN and dried LIQION (Nafion, Liquion 1105, Ion Power Inc.) in a ratio of 40:60 and 30:70 with a total solid concentration of 18% and 25%, respectively, were used. The solutions were then electrospun with the following conditions: Distance between aluminum foil grounded collector and needle tip (22 gage stainless steel needle, Hamilton Co.) was between 15 and 16 cm, applied voltage was around 9–10 kV, relative humidity inside the spinning setup was kept below 20% and the solution flow rate was set to 0.2 mL/h using a syringe pump (New Era Pump Systems, Inc.). After electrospinning, the mats were first stabilized in a convection oven at 280 °C for 6 h in air. The stabilized mats were carbonized in a tube furnace (MTI Corporation) at 1000 °C for 1 h (with a heating rate of 3 °C/min) under continuous nitrogen flow.

2.2. Fabrication of SDIB copolymer

To prepare the SDIB powder, 2.7 g sulfur (Sigma, 100 mesh) in a vial was melted at 180 °C (±2 °C) using an oil bath and was stirred using a magnetic stirrer. When the sulfur solution changed color from yellow to orange, 734 µL (0.675 g) 1,3-Diisoprpenylbenzene monomer (DIB, TCI) was added and stirred until the solution became very viscous. The sulfur to monomer ratio in this reaction was calculated to achieve a sulfur-rich copolymer with 20 wt% monomer (DIB) and 80 wt% sulfur. The copolymer was removed using a spatula and cooled down to room temperature in the fume hood. A glassy red block of solid material was obtained and grinded into a fine powder. As a reference, to better understand the effect of adding the DIB monomer, we synthesized heat-treated sulfur using the same procedure but without adding the DIB monomer. All the material characterization was carried out using the copolymer powder unless specified otherwise.

2.3. Physical characterization

To analyze the morphology and structure of the samples, scanning electron microscopy (SEM) (Zeiss Supra 50 VP) was used. For elemental mapping of the cathode energy dispersive spectrometer (EDS; Oxford) coupled with SEM device was utilized. Thermogravimetric analysis on sulfur powder, heat-treated sulfur, SDIB powder, and SDIB-miCNF cathode was carried out on a Q50 TGA (TA Instruments, New Castle, DE), under a steady flow (60/40) of N_2 and heating rate of 2.5 °C/min from room temperature to 700 °C. To analyze the pore shape, size, and volume for meCNF and miCNF samples, Nitrogen adsorption-desorption experiments were carried out at 77 K on an automated gas sorption analyzer (AutoSorb iQ2, Quantachrome Instruments). The samples were degassed at 200 °C overnight under vacuum, and NLDFT model was used to calculate the pore size and volume and samples. X-ray diffraction (XRD) was collected using a X-ray Diffractometer (Rigaku SmartLab) to analyze the crystal structure of the samples. The infrared spectra of the samples were collected using a Fourier transform

infrared (FTIR) spectrometer (Nicolet iS50, Thermo-Fisher Scientific) using an extended range diamond ATR accessory. A deuterated triglycine sulfate (DTGS) with a resolution of 64 scans per spectrum at 8 cm^{-1} was used and all the spectra were further corrected with background, baseline correction and advanced ATR correction in the Thermo Scientific Omnic software package. It should be noted the for postmortem FTIR study, we transferred the FTIR puck inside the glovebox and sealed the cycled cathode so that the cathode was not exposed to air during the FTIR experiment. The structure of the copolymer was confirmed by HNMR spectroscopy (500 MHz) using a Varian Unity Inova NMR systems spectrometer with [D]chloroform as solvent.

2.4. Li-S cells fabrication and electrochemical testing

SDIB powder and sulfur powder (for reference) were used as active material for cathode preparation. The miCNF and meCNF mats were dried overnight at 140 °C and punched into discs using a punch with area of ~0.855 cm^2. The weight of CNFs used in this study was controlled between 0.95 to 1.25 mg, and SDIB copolymer incorporated was 1.2 to 1.4 mg. Based on the weight measurement and TGA results, an absolute sulfur loading of 0.96 to 1.1 mg is achieved. The final sulfur loading on each cathode was 1.1 to 1.3 mg/cm^2 and 45–50 wt%. Ultra-rapid sulfur melt diffusion method was used to incorporate sulfur within the nanofibers, as introduced by our group previously [27]. Briefly, the desired amount of copolymer/sulfur was added on top of the punched nanofiber mats and sandwiched between two weighing papers and heat pressed at 155 °C by applying a slight pressure (pressure ≤200 psi). The heat press time was optimized based on SEM pictures, and 2 min and 50 s treatment were used for copolymer and sulfur, respectively. The cathodes were then flipped so that the copolymer/sulfur incorporated side was kept away from the separator and faced the coin cell. The CR2032 (MTI Corporation) coin-type cells, lithium foil anodes (Aldrich; 11 mm diameter), S/SIDB-cathodes, a polypropylene separators (Celgard 2500; 19 mm diameter), 3 layers of nickel foam (MTI Corporation) as spacer and 30 µL electrolyte were used to assemble the Li-S battery cell in a argon-filled glove box (<1 ppm O_2 and H_2O). The electrolyte used in all coin cells was consisted of a 1.85 M $LiCF_3SO_3$ (Acros Organics) as salt, 0.1 M $LiNO_3$ (Acros Organics) (as an additive) and a mixed solution of 1,2-dimethoxyethane (DME, Acros Organics) and 1,3-dioxolane (DOL, Acros Organics) at a 1:1 vol ratio as solvents. All Li-S coin cells were rested for 6 h before electrochemical testing to equilibrate. After resting, the cells were conditioned at C/10 for (two cycles) and C/5 (one cycle) (where 1C = 1675 mAh/g) and then cycled at C/2 rate. Similarly, the cells cycled at C/5 were conditioned at C/10 for two cycles. Prolong cycling experiments were performed using a MACCOR (4000 series) battery cycler at different C-rates between 1.8–2.7 V. Cyclic voltammetry (CV) tests at different scan rates from 1.8 to 2.6 V was carried out using a potentiostat (Gamry reference 1000).

3. Results and discussion

The sulfur-rich copolymers were synthesized using inverse vulcanization technique. In brief, 2.7 g sulfur powder was heated to 185 °C to open the S_8 rings. Then, 734 µL 1,3-diisopropenylbenzene was added to the melted sulfur and stirred until the reaction was completed (details in experimental section). After cooling down to room temperature, a glassy red copolymer was obtained, which was further grinded into a fine powder. The weight ratio between the sulfur and DIB monomer in the reaction was 80:20 wt%. Rheological measurements and solid-state NMR studies in literature attempted to calculate the sulfur rank between the DIB monomer units [29,30]. Rheological measurements show that using this weight ratio, there is ~10 bridging sulfur between the DIB units [29]. Based on the study in reference 29, the sulfur rank changes form ~10 to ~1, as the monomer wt% increases from 20% to 65%. Moreover, the average sulfur bridging rank between the DIB units can be calculated assuming that the reaction between sulfur and DIB monomer is completed. This average sulfur rank (n) is calculated based on the wt ratio of monomer to sulfur ($\frac{mw_{DIB}}{n\times 32+n\times 32} = \frac{20}{80}$, where mw_{DIB} is the molecular wight of the DIB monomer), resulting in an average sulfur rank of 9.89 which is close to the reported values from literature.

To study the effect of porosity of CNFs on the cycling and capacity of Li-S cells, two different porous samples were designed using the PAN: Nafion weight ratio as 4:6 (miCNF) and 3:7 (meCNF). Electrospinning method followed by heat treatment was used to prepare these freestanding porous CNF mats. Fig. 1a and b show the SEM picture of the electrospun miCNF and meCNF fibers after thermal treatment. The SEM picture shows that fibers exhibit a smooth surface with interfiber voids (macrostructure). The average diameter of the fibers for miCNF and meCNF is 279 and 266 nm (measured using Image J software), respectively. The Brunauer–Emmett–Teller (BET) N_2 gas adsorption-desorption and pore size distribution for the porous CNF samples is given in Fig. 1c and 1d. As shown in the figure, both the miCNF and meCNF nanofiber samples exhibit type IV isotherms, where the amount of adsorbed N_2 gas slowly increases at relatively high pressure. The hysteresis that appeared at a relative pressure between 0.4 to 0.6 confirms the presence of slit-shaped mesopores in both samples [25,26,31].

To determine the surface area, total, micropore and mesopore volume of the samples N_2 desorption at 77 K was used, and a density functional theory (NLDFT) model was employed. Fig. 1d shows the pore size distribution of miCNF and meCNF samples. From the figure, it is clear that both samples have a similar amount of micropore size and volume. However, although both the miCNF and meCNF samples have similar mesopore size of around 2–4 nm, the meCNF sample has a significant amount of mesoporosity that is larger in diameter (>5 nm) which is absent in the miCNF sample. In other words, the mesopore structure of the meCNF sample ranges from 2 to 7 nm where the miCNF sample has the mesopore size from 2 to to 5 nm only. The porosity of both samples is from decomposing Nafion as a sacrificial polymer, as reported in our previous work [25]. As mentioned before, using the density functional theory model, total pore volume for miCNF and meCNF samples is ~0.773 cm^3/g and ~0.467 cm^3/g, respectively (see table 1). While meCNF has larger mesopores compared to miCNF samples, the mesopore volume of two samples is calculated to be 0.502 cm^3/g and 0.275 cm^3/g, respectively, which shows that despite having a similar microporous structure, the mesopore volume and size is considerably higher in meCNF samples. Moreover, the freestanding nature of the fibers eliminates the need for a binder and allows a better comparison and study on the effect of porosity, since the binders can significantly affect the morphology and pore structure of the sample [27].

In order to characterize the sulfur-rich copolymer, HNMR was used to confirm the formation of the C-S bond from inverse vulcanization and to prove the existence of aromatic and aliphatic functional groups from the DIB monomer. Fig. 2a shows the HNMR spectrum of the SDIB copolymer using chloroform D as solvent. The peaks at 7.27 ppm and 1.57 ppm correspond to -chloroform and water [32]. The peaks at 6-8 and 1–2 ppm (except for 1.57 ppm) is because of the presence of an aromatic ring and methyl protons in the structure of the copolymer [19]. Moreover, the resonances between 2.9 and 3.4 ppm are from the methylene peaks present in DIB monomer backbone that are bonded to the sulfur units. As it can be seen, the peaks from methylene protons

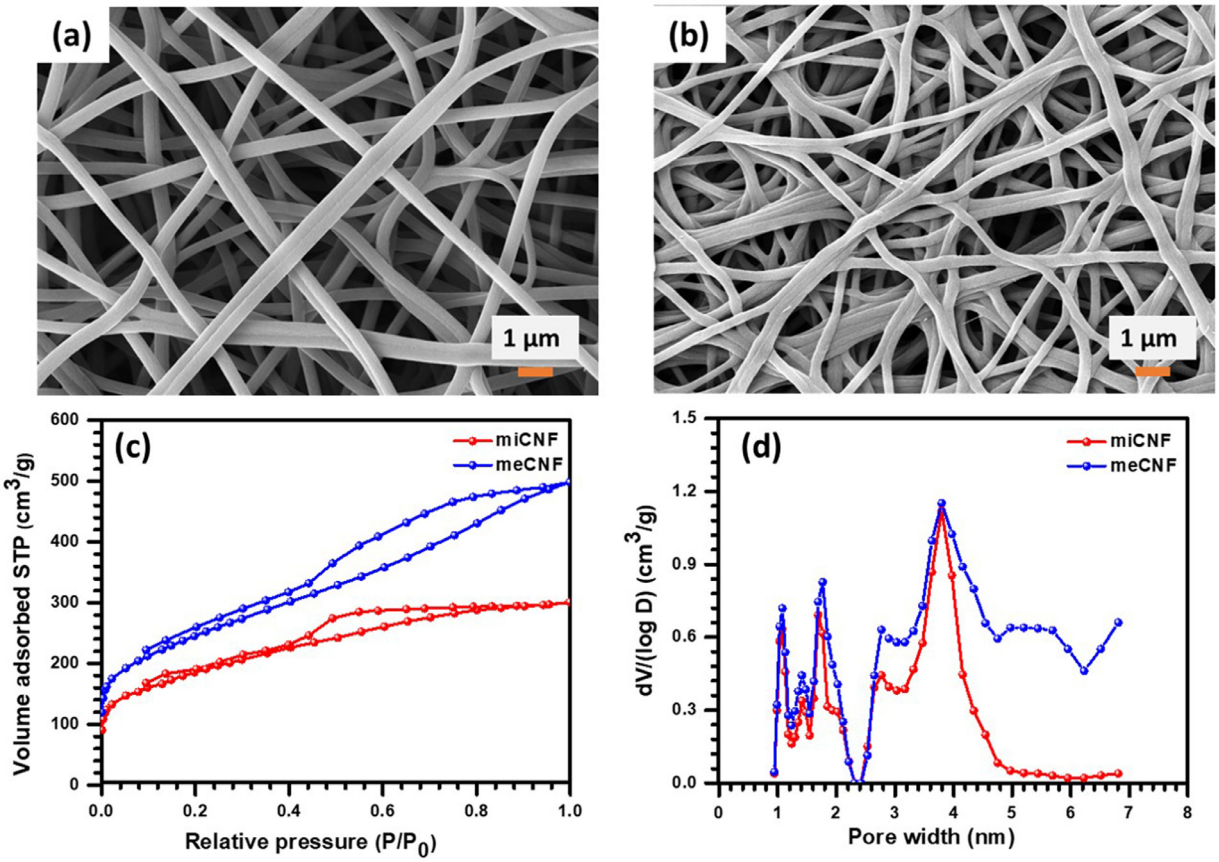

Fig. 1. SEM images of a) meCNFs and b) miCNFs; c) BET N_2 adsorption-desorption curves and d) Pore size distributions for meCNFs and miCNFs.

Table 1
Parameters of porous surface area and pore volume for meCNF and meCNF.

Sample	BET surface area (m^2 /g)	V_{total} (cm^3/g)	V_{micro} (cm^3/g)	V_{meso} (cm^3/g)
meCNFs	674.5	0.773	0.271	0.502
miCNF	641	0.467	0.192	0.275

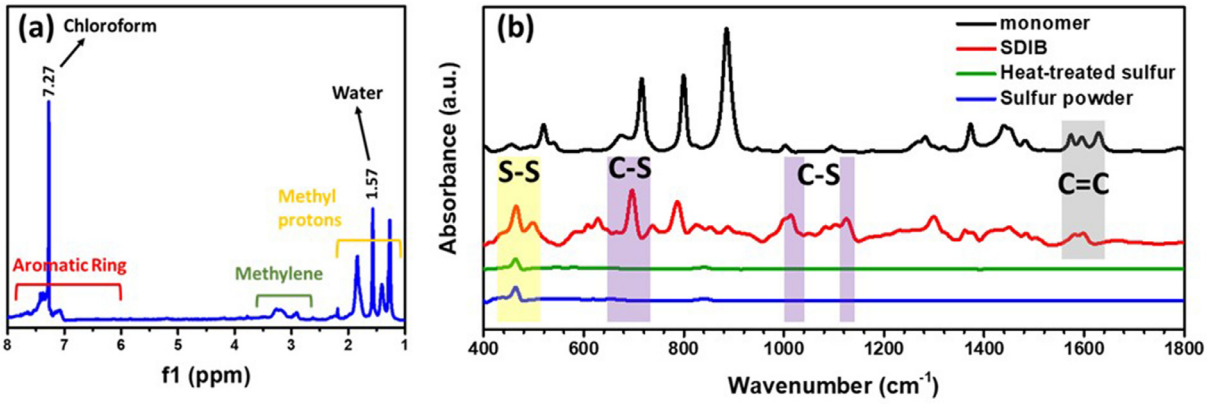

Fig. 2. a) HNMR spectra for SDIB copolymer; b) FTIR spectra of the sulfur powder, SDIB copolymer, and heat-treated sulfur which is molten sulfur, cooled from 180 °C to room temperature without adding DIB monomer.

are shifted to the higher side as a result of C-S bond formation [29].

To better understand the structure of the sulfur-rich copolymer, Fourier-transform infrared spectroscopy (FTIR), was carried out for four samples (i.e., sulfur powder, heat-treated sulfur, DIB monomer, SDIB copolymer) and the results are shown in Fig. 2b. The heat-treated sulfur used in FTIR, TGA and XRD experiments, is synthesized by increasing the temperature of the sulfur powder until an orange/light red color is achieved, followed by cooling the viscose liquid to room temperature. Heat-treated sulfur can be used as a reference for characterization because the synthesis method is the same as SDIB copolymer without the addition of DIB monomer. In this figure, the peaks at 464 cm^{-1} and 843 cm^{-1} are assigned to the stretching vibrations of S-S bond in sulfur powder and heat-

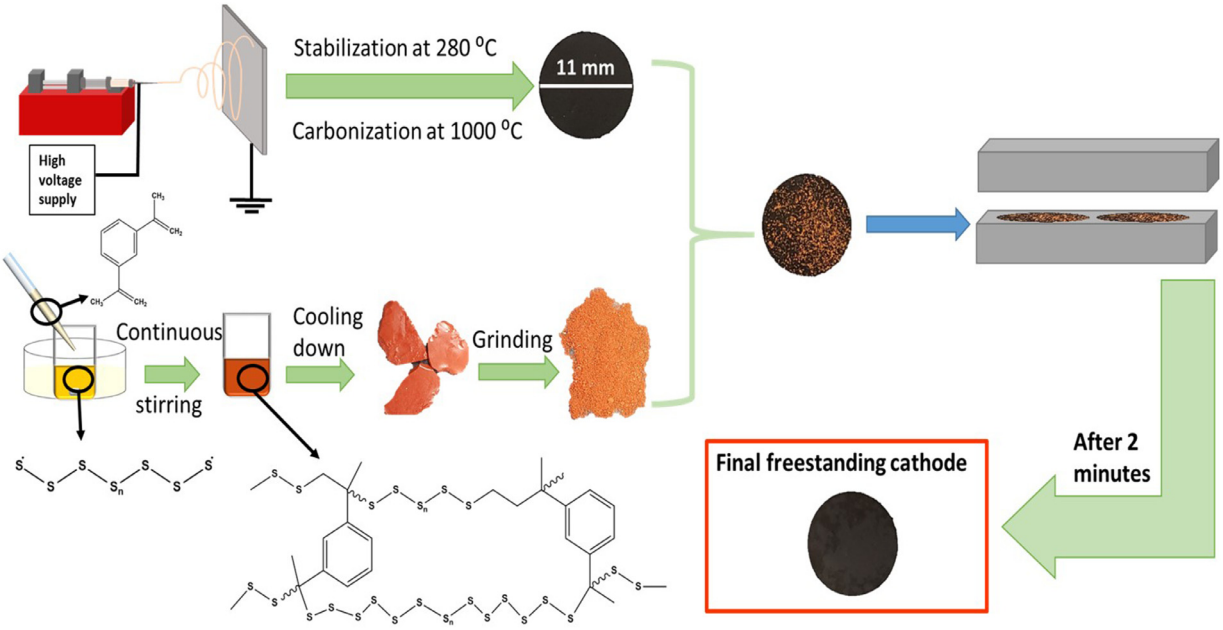

Schematic 1. Synthesis scheme of the SDIB copolymer and the fabrication process of the SDIB-miCNF and SDIB- meCNF cathodes.

treated sulfur [33,34]. By comparing the IR spectra of sulfur powder and heat treated sulfur, it is clear that sulfur heat treatment did not change the S-S peak position in the IR spectrum. The assigned S-S peak was shifted to 465 cm^{-1} in SDIB copolymer, and another peak appeared at 498 cm^{-1}. We believe that the appearance of the new peak originated from the vibrations of the S-S bond attached to the carbon in the copolymer. The shift might be because of the existence of the higher chain length polysulfides in the polymer [35]. Based on previous reports, C-S stretching bond in organosulfur compounds appears between 600–800 cm^{-1} [35-37]. There are also some studies where they have shown the existence of this peak between 1000 and 1200 cm^{-1}. In SDIB copolymer, the strong peak at 696 cm^{-1}, and 1013 and 1125 cm^{-1} are assigned as C-S stretching bond in sulfur-rich copolymer [38]. It should be noted that these peaks are absent in the IR spectrum of the DIB monomer and they are similar to the previously reported C-S bond in literature [38,39]. The peaks at 1582 and 1589 cm^{-1} in SDIB copolymer are related to the existence of C=C and shows that there is a trace of unreacted monomer in the synthesized copolymer [40]. The appearance of the three peaks, at 696 cm^{-1}, and 1013 and 1125 cm^{-1}, in the IR spectrum of the SDIB, further confirms the formation of the C-S bond in the inverse vulcanization reaction.

Schematic 1 shows the synthesis schematic for preparing SDIB-miCNF, SDIB-meCNF cathodes. We used ultra-rapid melt diffusion technique to infuse the sulfur-rich copolymer (SDIB) powder into the punched CNF mats [27]. In this technique, desired amount of SDIB powder is sprinkled on mi/meCNFs and heat pressed at 155 °C for 2 min by applying a slight pressure (<200 psi) in a hydraulic heat-press. This technique allows us to incorporate the SDB copolymer into the CNF mat in only 2 min, avoiding the complicated and long processes that are often used in literature. Moreover, it enables us to achieve a controlled SDIB loading (based on the amount of sprinkled SDIB before heat press) and reduce the amount of time and energy otherwise used in reported studies such as melt diffusion, vacuum infiltration and solvent evaporation in slurry processing. Fig. 3a shows the SEM image and elemental mapping of the cathodes after SDIB incorporation. As can be seen in this figure, SDIB copolymer is deposited on the nanofiber and between the fibers, as well. Also, it is shown in elemental mapping that the sulfur is well distributed on the cathode. Thus, the macroporous structure of the CNF mat facilitates the very rapid incorporation of the SDIB powder (in only 2 min) and, provides space to accommodate the volume change of the active material upon charging and discharging the battery (lithiation and de-lithiation).

The freestanding nature of the fibers eliminates the need for polymer binders and heavy current collectors. In conventional cathodes, binders are considered as dead weight added to the cathode which has a negative impact on battery performance by increasing the internal resistance and lowering the energy density [41]. Moreover, as a part of eliminating conventional slurry processing, there would be no need to use N-methyl-2-pyrrolidone (NMP) solvent which is known to be a reproductive and developmental toxin [42].

Fig. 3b shows the thermogravimetric analysis (TGA) curves for sulfur powder, heat-treated sulfur, SDIB, and SDIB-miCNF cathode. The sulfur powder shows a steep weight loss between 150 and 245 °C and the heat-treated sulfur is slightly shifted to the left. The very small decrease in decomposition temperature of the heat-treated sulfur compared to the sulfur powder might be because of the ring opening polymerization of elemental sulfur (S_8), which results in the formation of long chains, hence, requires lower energy for decomposition. SDIB sample shows the same weight loss pattern as the sulfur powder and heat-treated sulfur. Based on the TGA result, the formation of C-S bond in sulfur-rich copolymer did not change the thermal stability of sulfur in SDIB copolymer. Moreover, TGA curves confirm the formation of SDIB copolymer in a ratio of 80:20 (sulfur:DIB) wt%. After SDIB incorporation on miCNF, sulfur decomposition started at lower temperatures (compared to the SDIB). The decrease in decomposition temperature after heat treatment could be attributed to the increased surface area of the SDIB copolymer incorporated to the CNF mat, which results in more efficient heat transfer in TGA [43]. Our lab reported a similar trend when sulfur powder was incorporated (as active material) using ultra-rapid melt diffusion method [27]. Moreover, from the TGA curves, we can also conclude that the SDIB particles are distributed on the nanofibers and within the macroporous structure of the CNFs. The single weight loss profile confirms that SDIB active material is not incorporated inside the micropores of the miCNF nanofiber [15]. XRD was performed to investigate the

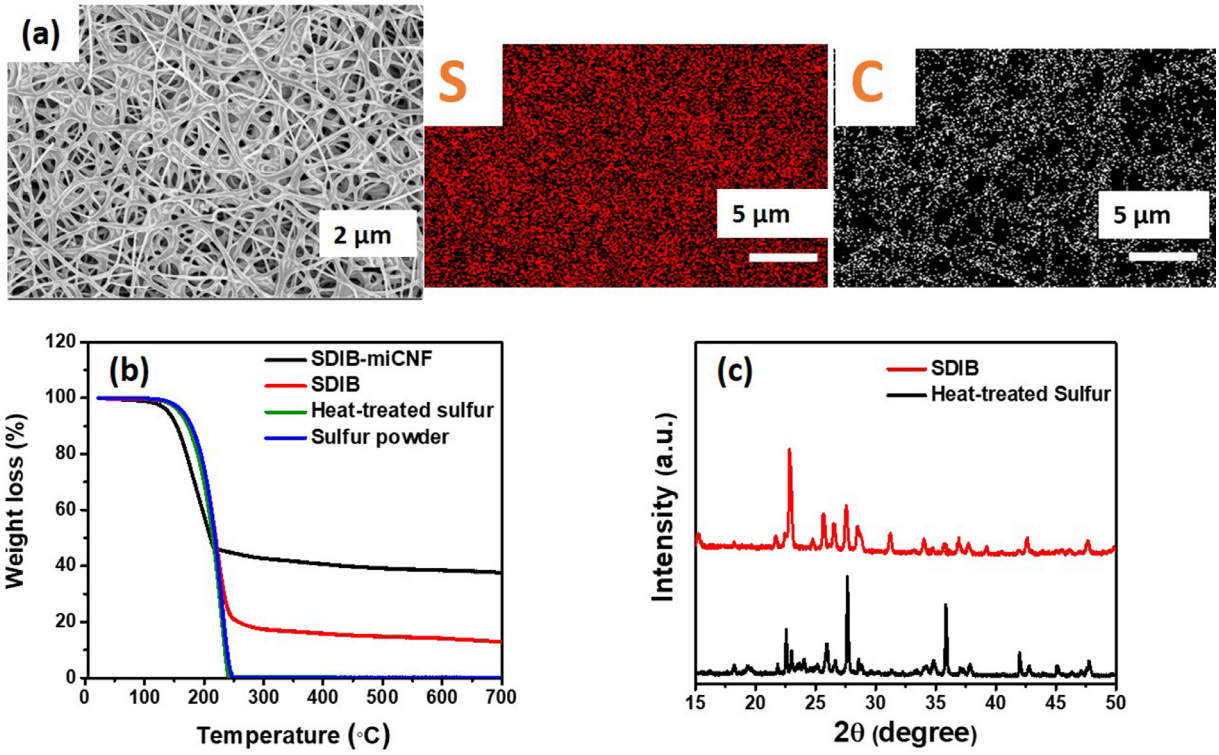

Fig. 3. a) SEM image and elemental maps for SDIB-miCNF cathode, b) TGA curves of the sulfur powder, heat-treated sulfur, SDIB, the SDIB-miCNF cathode and c) XRD results for heat-treated sulfur and SDIB copolymer, heat-treated sulfur is molten sulfur cooled from 180 °C to room temperature without adding DIB monomer.

crystal structure and possible phase change of sulfur after the ring opening reaction. As depicted in Fig. 3c, the XRD pattern for heat-treated sulfur and SDIB powder are very similar to the pure sulfur. This indicates that the ring opening reaction of the sulfur did not change the sulfur phase and the orthorhombic structure of sulfur still exists. Moreover, the SDIB powder retains the crystalline structure after covalent C-S bond formation, which can be supported by the existence of pure sulfur peaks (at ~23, ~26, ~28 and ~29 degrees) in XRD pattern of the SDIB copolymer [19,38]. The similarity between the XRD pattern of elemental sulfur and SDIB copolymer powder suggests the existence of sulfur crystalline domain in SDIB copolymer or existence of some unreacted sulfur embedded in the SDIB copolymer [44,45]. Diez et al. showed the existence of a melting peak in the first heating cycle of the DSC experiment [46]. The observed small peak in the DSC curve was attributed to the existence of a trace amount of unreacted sulfur embedded in the SDIB copolymer. Based on the PXRD and DSC results of the SDIB copolymer, the authors concluded that the unreacted sulfur exists in a very small amount. Moreover, Wadi et al. demonstrated the partial depolymerization of SDIB at concentrations of DIB< 30 wt% [38]. The reason behind the depolymerization and formation of the loose sulfur was attributed to the formation of the long chain sulfur, and incomplete termination with the cross linker (DIB units here). Based on the XRD results shown in Fig. 3c, we expect the presence of a small amount of unreacted sulfur in the SDIB powder.

For electrochemical testing, we prepared SDIB-miCNF, SDIB-meCNF cathode materials using rapid melt diffusion technique. 2032 coin-type Li-S cells were fabricated using the cathodes without addition of any binders and current collectors (details are in the experimental section). Fig. 4a shows the cyclic voltammetry (CV) curves of the SDIB and sulfur on miCNF at a scan rate of 0.1 mV/s. The CVs of the cathodes showed two reduction peaks (cathodic peaks) and a broad oxidation peak (anodic peak), confirming the reversibility of the active material used in cathodes. The two reduction peaks in S-miCNF at ~2.29 and ~1.95 V correspond to the formation of higher and lower order polysulfides and deposition of the end product (Li_2S_2 and Li_2S), respectively. On the other hand, the broad anodic peak centered at ~ 2.4 can be attributed to the reformation of the elemental S_8 from reduced discharge products (Li_2S_2 and Li_2S). Similarly, for SDIB-miCNF cathodes, two cathodic and one broad anodic peak were observed. The two reduction peaks correspond to the formation of higher and lower order lithium polysulfides along with the lithium organo-polysulfides and the observed broad peak, shows the reversible oxidation of the discharge products, back to the elemental sulfur and organo-sulfur copolymer [47]. The comparison between the CVs of SDIB-miCNF and S-miCNF shows that the SDIB and elemental S_8, exhibit very similar electrochemical reversibility and behavior. The similarly in cyclic voltammetry could be due to the presence of unreacted loose sulfur present in the initial material and/or due to the long sulfur chain length within the DIB units resulting in minimal effect on peak voltages as also seen in previous literature reports [19,20,22,36]. However, a slight shift in the reduction and oxidation shift can be seen in the figure. The reduction peak of the SDIB- miCNF shows slightly lower onset potentials compared to the S-miCNF cathode. A similar trend can be seen in the oxidation peak, where the anodic peak in SDIB-miCNF is shifted to a lower potential. The lower onset potential for the oxidation peak might arise from the better re-utilization of the solid state and insulating end products (i.e., lithium polysulfide and lithium organopolysulfide). It has been reported that the SDIB copolymer has a "plasticizing" effect, which enhances the deposition and re-utilization of the Li_2S [17]. The Li_2S final product has high activation energy, and it is hard to be reused during the oxidation because of the non-uniform distribution and aggregation on the electrode surface. The large Li_2S particles would eventually lose their electrical contact with carbon and therefore cannot be reused, which results

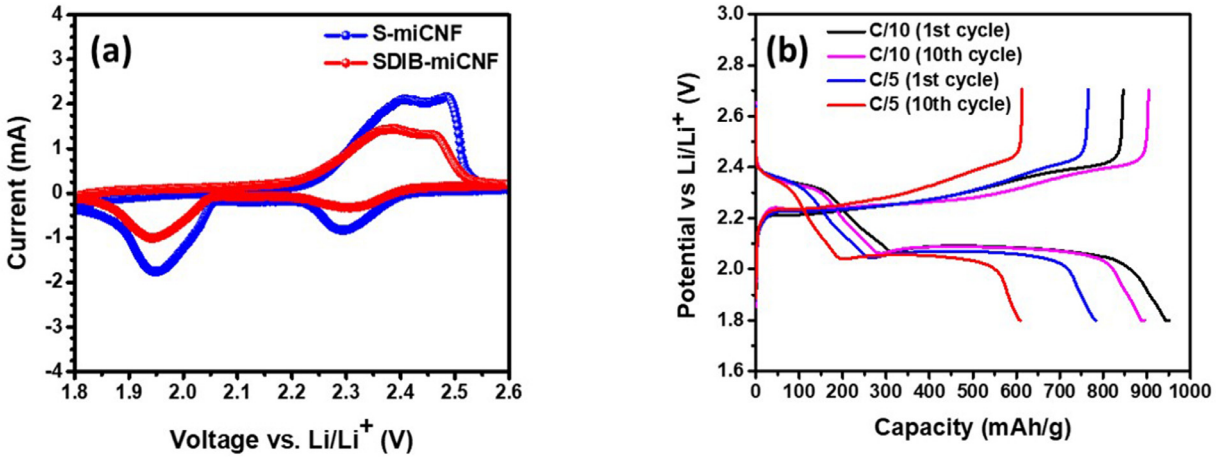

Fig. 4. a) CV curves of the SDIB-miCNF and S-miCNF cathodes b) Charge–discharge profiles for SDIB-miCNF at different rates (C/10 and C/5).

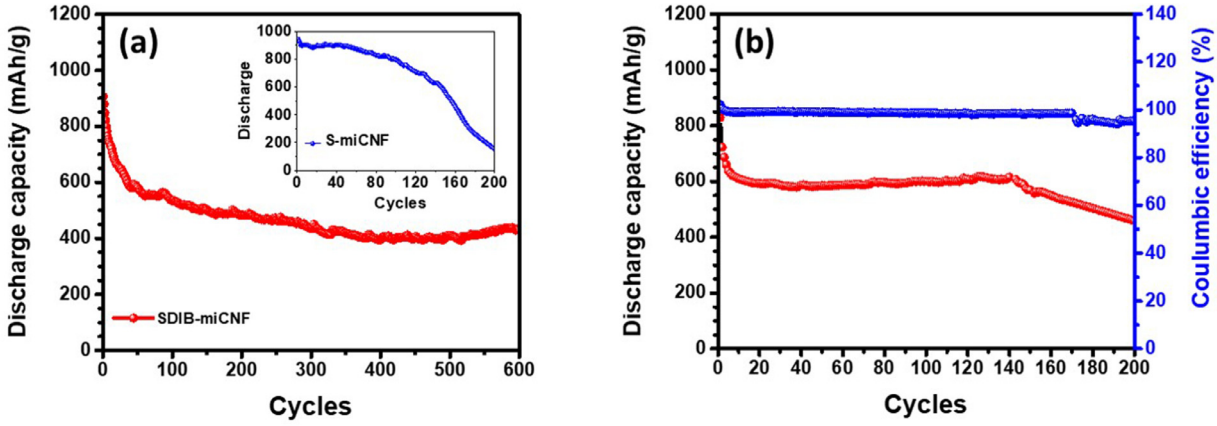

Fig. 5. a) Long term cycling at C/2 rate for SDIB-miCNF and S-miCNF (inset) b) Long term cycling (in red) and coulombic efficiency (in blue) at C/2 rate for SDIB-meCNF.

in loss of active material and high internal resistance in the battery [48,49]. Therefore, improved re-utilization of the insulating end products can have a tremendous effect on the coulombic efficiency of the battery. This phenomenon is shown to have a high impact on the cycling of lithium-sulfur batteries, and it is known as the catalytic effect of the metal oxides and other additives/host material on the performance of the battery [50].

Fig. 4b shows the Charge- Discharge profiles of the SDIB-miCNF cathode material at different cycles evaluated at two different C rates. Two clear voltage plateaus at ~2.3 V and ~2.1 V are present in the discharge curves. The existence of these plateaus is attributed to the two-step reduction of the solid-state sulfur-rich copolymer higher order organo-polysulfides and then to the solid-state end products (oragno lithium polysulfide and oragno lithium sulfide), consistent with two reduction peaks shown in CV curves. Comparing the charge-discharge curves at different scan rate, we can conclude that at higher discharge rate (when higher current is applied) the cathode polarization and the voltage hysteresis between two curves increase [51].

Long-term cycling of the SDIB-miCNF and reference S-miCNF at C/2 was carried out keeping all parameters such as electrolyte amount, separator, etc. identical. For cycling at C/2 rate, all the cells were conditioned at C/10 for 2 cycles and at C/5 for 1 cycle. The cycle life of the SDIB-miCNF and S-miCNFis compared in Fig. 5a. As can be seen in this figure, S-miCNF has a higher capacity, but SDIB-miCNF exhibits better cycle life. The higher capacity of S-miCNF compared to SDIB-miCNF can be explained by the formation of organo-polysulfides in SDIB-miCNF, wherein one Li^+ ion reacts with the organosulfur (C-S-S_n-Li). On the other hand, when sulfur is used as the active material, polysulfides are formed when two Li^+ ions react with sulfur (Li-S_n-Li). Despite the lower capacity, SDIB-miCNF shows a long cycle life (600 cycles compared to 100 cycles in S-miCNF). The SDIB-miCNF cathode exhibited an initial capacity of ~905 mAh/g, which was stabilized to close to 600 mAh/g after 50 cycles. This capacity value remained stable with a very small capacity decay rate of 0.046% per cycle and coulombic efficiency of more than 98% throughout the 600 cycles. This is possibly due to the C-S bond formation that binds the polysulfides chemically by forming organo-lithium polysulfides and reduces the shuttle effect. We believe when discharging the SDIB-miCNF cell, the -S-S_n-S- bond present in sulfur-rich copolymer breaks and sulfur with different chain lengths are formed. This process takes place in each cycle, and the loose sulfur (i.e., unreacted or not bonded to carbon in sulfur-rich copolymer) are being formed gradually with cycling (see Schematic 2). Note that the origin of this loose sulfur could be due to two reasons 1) unreacted sulfur, 2) formation of loose sulfur during each cycle due to S-S bond breakage in SDIB. On the other hand, in S-miCNF, all the active material is in the form of S_8 ring and can react and form the polysulfide immediately, once it is in contact with the electrolyte. We believe that the slow rate polysulfide formation in SDIB-miCNF results in more effective polysulfide adsorption by micropores of the miCNF host. Hence, despite having the same host material and pore structure, the capacity of the SDIB-miCNF cathode remains stable, while the capacity of the S-miCNF drops in less than 100 cycles.

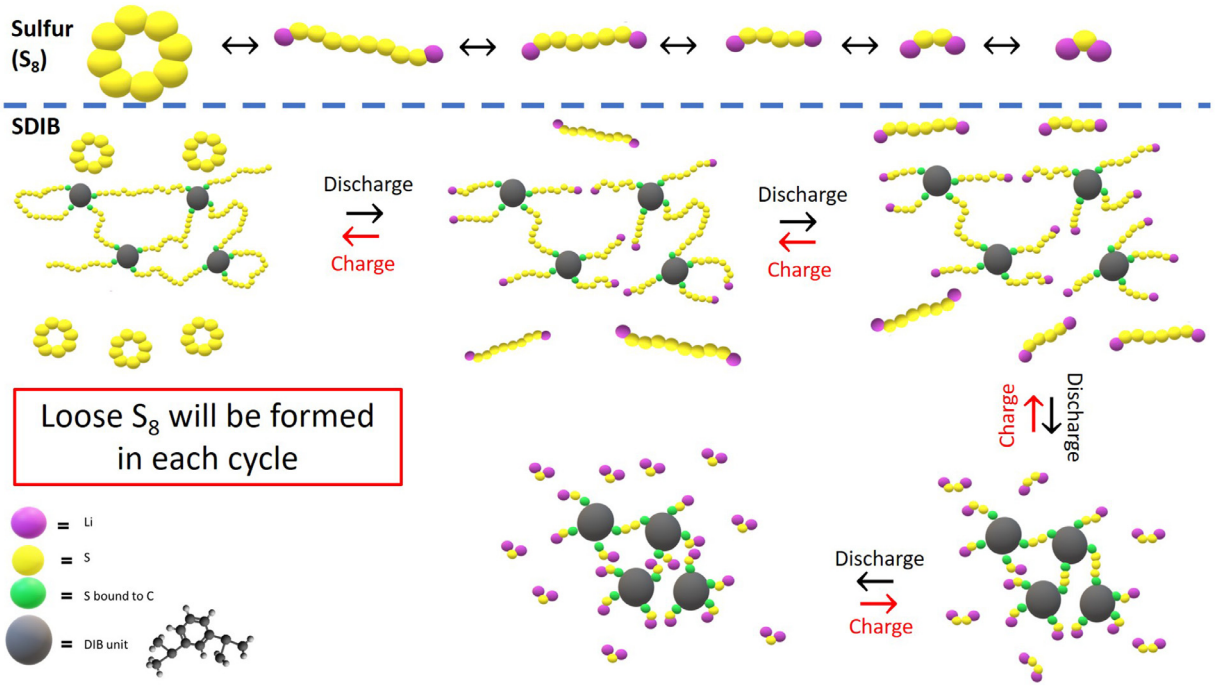

Schematic 2. Comparison between the reaction mechanisms of sulfur cathode and SDIB cathode.

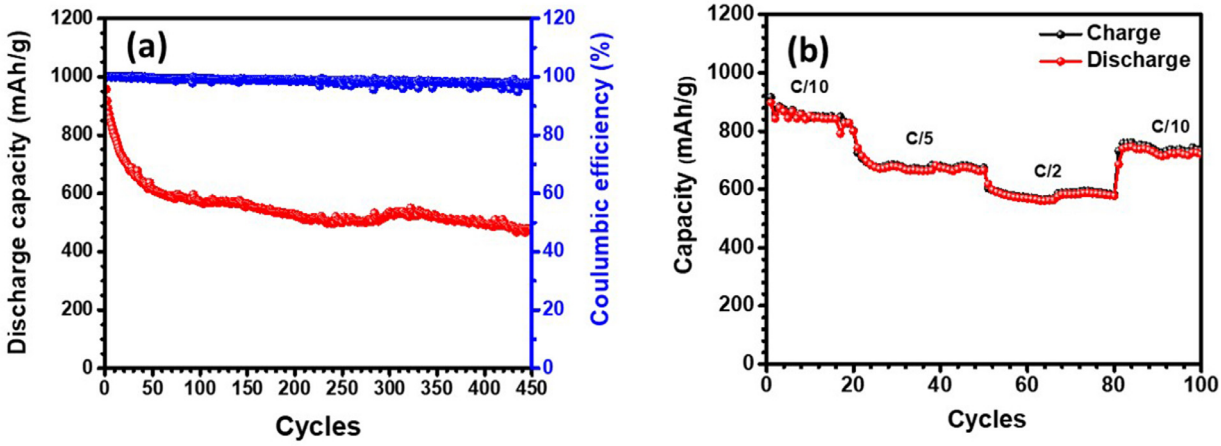

Fig. 6. a) Long term cycling and coulombic efficiency for SDIB-miCNF at C/5 rate and b) Rate performance at different C-rates for SDIB-miCNF.

To investigate the effect of carbon nanofiber porosity, meCNFs were used as host material, because of the larger mesopore size and volume but similar micropore volume compared to miCNF (as shown in BET results). We initially hypothesized that the larger pore size of the meCNF would result in higher capacity (because of the better electrolyte/active material contact) while, the higher cycle life will be maintained because of the microporous structure. Fig. 5b shows SDIB-meCNF cathode performance. As expected, the SDIB-meCNF cathode exhibited higher capacity which confirms the higher sulfur utilization as a result of higher surface area and larger mesopores provided for electrolyte (Li^+ ion) diffusion [52]. However, despite the higher sulfur utilization, the cycle life of the cathode decreases significantly after 145 cycles. The SDIB-meCNF cathode showed a stable capacity of 600 mAh/g but the stable capacity lasted for 145 cycles only. However, the capacity decreases to 450 mAh/g after 200 cycles and coulombic efficiency is further decreased to 95%. The obtained results show that the larger mesopore size and volume in meCNF sample acts as a two-edged sword; On one side, the capacity increases because of the high sulfur utilization. On the other side, the lithium polysulfides can easily escape from CNFs because of the larger pore size provided. Hence, although meCNFs has a microporous structure similar to the miCNF, but, the larger mesopores results in higher polysulfide shuttle in SDIB-meCNF cells. Our finding that optimally-sized pores are essential to maintain cycling stability further suggests that there is indeed loose sulfur and polysulfides in our system. As discussed before, this loose sulfur could comprise of both unreacted sulfur in the initial material and additional loose sulfur formed during cycling.

Fig. 6a shows the cycling stability of SDIB-miCNF at C/5 rate. As it can be seen in this figure the capacity decreases to ~572 mAh/g in first 100 cycles, but delivers a very stable capacity of ~520 mAh/g after 350 cycles (capacity retention of 91% from 100 to 350 cycles) and ~480 mAh/g after 450 cycles with coulombic efficiency being >97% throughout. Moreover, the rate capability test was carried out and the SDIB-miCNF cathode was cycled at C/10, C/5, C/2 and C/10 for 20, 30, 30 and 20 cycles, respectively. Fig. 6b shows that the cathode exhibits a high discharge capacity of ~920

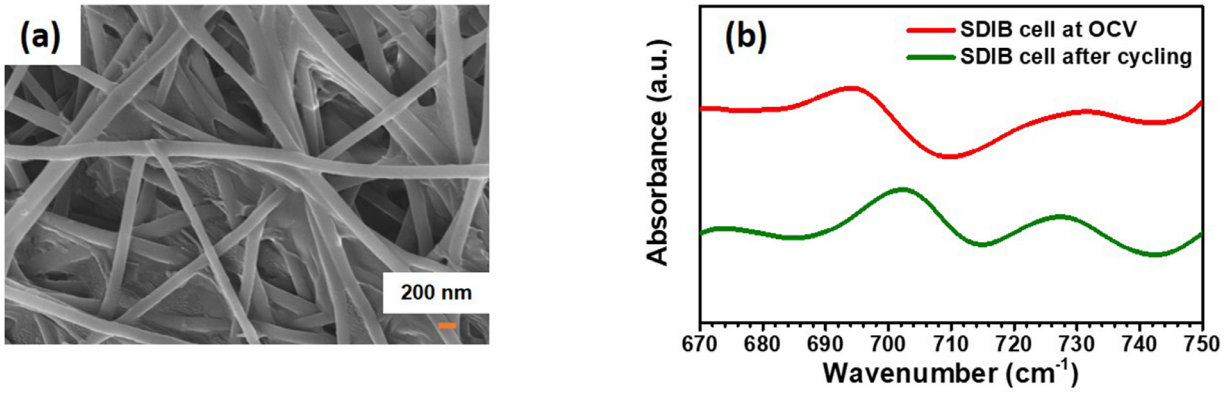

Fig. 7. postmortem a) SEM and b) FTIR studies of the SDIB cathode after cycling.

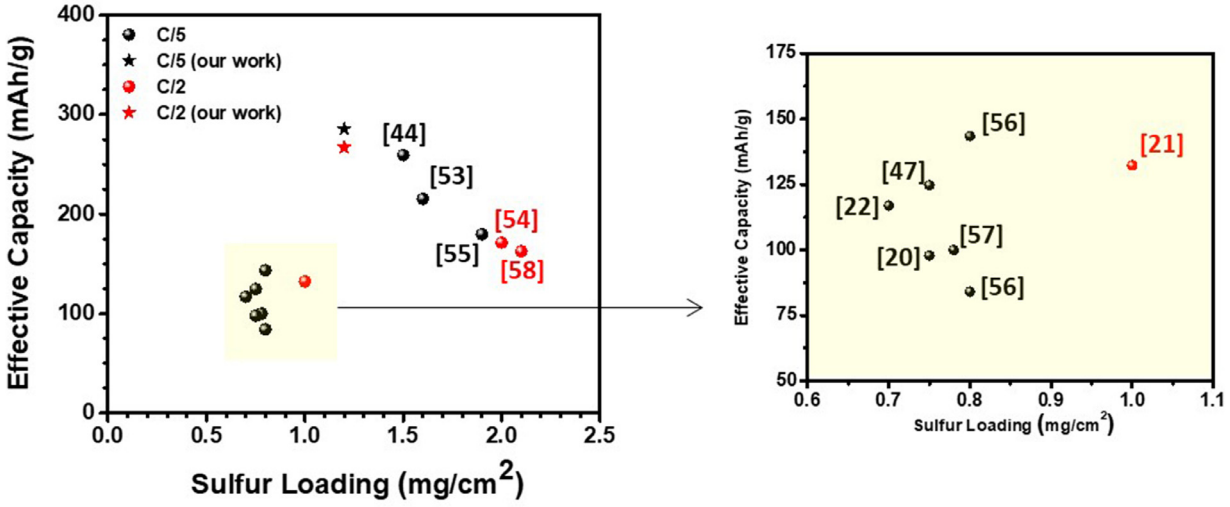

Fig. 8. Effective discharge capacity after 100 cycles accounting for total electrode weight in the cathodes reported in literature compared to our work at C/2 and C/5 (data presented using ⋆ is the result of present study).

mAh/g at first C/10 cycles, which decreases to ~800 mAh/g after 20 cycles. Moreover, a stable capacity of ~664 mAh/g after 30 cycles at C/5 and a capacity of ~577 mAh/g after 30 cycles at C/2 was achieved. Also, it can be seen that after cycling at different C-rates, the SDIB-miCNF cathode reached the capacity of ~747 mAh/g at C/10.

The structural integrity of the SDIB-miCNF cathode material after long-term cycling is shown in Fig. 7a. It is clear from the picture that the SDIB-miCNF cathode preserved the continuous carbon fiber structure even after long term cycling. The postmortem SEM picture shows that the freestanding CNF mat can serve as a host material in cathodes and can provide continuous electron pathways. Moreover, the preserved structure of the CNF, as well as the existence of the copolymer between fibers, show that the macroporous structure of the CNFs can accommodate the volume expansion of the cathode upon cycling. Fig. 7b shows the FTIR spectrum of the discharged cathode before (at OCV) and after cycling (at fully discharged state). It is clear from this figure that the C-S bond (located at ~700 cm^{-1}) is present before and after cycling. This result shows that the C-S bond does not break during cycling, However, it shifts to higher order wavenumbers as a result of organo-lithium polysulfide formation.

To understand the effect of the freestanding nature of our cathode material we provide a mathematical method to analyze and compare the powdered based cathode material from literature with our freestanding SDIB-CNF cathodes. To make a comparison, we calculated the effective capacity values based on the total weight of the cathode used in a battery. It is important to note that in the real applications, the energy density of a battery plays a vital role and the energy density should be calculated using the total weight of the cathode material in a battery (i.e., binders, conductive additives, current collectors and active material). In this regard, calculating the effective capacity of a cathode helps us have a better understanding of the capacity values reported in literature. To calculate the effective capacity, we used discharge capacity of the batteries based on powdered sulfur rich copolymers after 100 cycles [20-22,44,47,53-58]. The following equation was used for the effective capacity calculation:

$$C_{eff} = \frac{C_s \times w_s}{w_t} \quad (1)$$

Where C_{eff} is the effective capacity in mAh/g, w_s is the sulfur weight in cathode (mg), and w_t is the total weight of the cathode (mg) calculated using the equation below:

$$w_t = \frac{w_s \times 100}{f_s} + A_c \times 4 \quad (2)$$

In this equation, f_s is the sulfur weight percent in cathode, A_C is the area of the cathode (cm^2) reported in each study. The first term in this equation represents the weight of the powder-based cathode, which includes the active material (the sulfur-rich copolymers used), conductive material and insulating binder. The second term in Eq (2) accounts for the weight of the Al current collector

used in the cathode fabrication. Weight of the current collector is reported to be 3– 5 mg/cm^2 [59,60] so, for the sake of comparison, we assumed this weight to be 4 mg/cm^2 in all the studies. Fig. 8 shows the effective capacity of our freestanding cathode and some of the results reported in literature where sulfur-rich copolymer powdered based cathodes are used. As it can be seen in this figure, our freestanding cathode material offers higher effective capacity compared to other powdered based cathode materials.

Conclusions

In our work, we study and develop freestanding, binder and current collector-free electrospun nanofibers as a platform to understand the role of host porosity in sulfur-rich copolymer-based Li-S batteries. Based on the XRD results presented, the SDIB copolymer is expected to have some unreacted residual sulfur. To understand the effect of porosity two different samples (miCNF and meCNF) were fabricated using electrospinning technique. When miCNF was used as a host material, after an initial drop within 50 cycles, the capacity remained stable up to 600 cycles with a small capacity decay rate of 0.046% per cycle. On the other hand, SDIB-meCNF cathode delivered a stable capacity of ~600 mAh/g with negligible decay for 145 cycles only. Additionally, the control/reference cell with sulfur as the active material (miCNF as host) showed a rapid decay in capacity in less than 100 cycles suggesting a clear advantage of sulfur-rich copolymers as active material (over pure loose sulfur) due to the presence of C-S bond leading to chemically bound soluble polysulfides. Based on the electrochemical results obtained, we believe that the porosity of the cathode host plays a significant role. This is because of the emergence of loose soluble -S_n- chains which arises from the S-S bond breakage in C-S-S_n-S-C when the battery is cycled as well as from unreacted residual sulfur in the original cathode. Slower polysulfide formation rate in SDIB-miCNF compared to S-miCNF results in effective polysulfide adsorption by micropores in SDIB-miCNF cathodes leading to substantial enhancement of cycling stability. We believe that as the pore size and volume increase in meCNFs, the electrolyte accessibility enhances, which results in relatively higher capacity. However, this also potentially leads to easier escape of polysulfides and early capacity fade in SDIB-meCNF based Li-S cells. Based on our results, engineering an efficient pore structure and introducing functionalities to the host material is required to obtain higher cycling even when sulfur rich copolymers are used as active material in Li-S batteries.

Associated Content

The authors declare no competing financial interests.

Author Contributions

The manuscript was written through the contributions of all authors. All authors have approved the final version of the manuscript.

Funding Sources

This work was supported by the National Science Foundation (CMMI-1537827, CMMI-1938787).

Declaration of Competing Interest

The authors declare that they have no known competing financial interests or personal relationships that could have appeared to influence the work reported in this paper.

Credit authorship contribution statement

Ayda Rafie: Investigation, Formal analysis, Writing - original draft, Conceptualization, Writing - review & editing. **Arvinder Singh:** Investigation, Writing - review & editing, Supervision. **Vibha Kalra:** Conceptualization, Supervision, Funding acquisition, Writing - review & editing.

Acknowledgment

Authors acknowledge Dr. Gogotsi and Dr. Seredych for BET measurement, Dr. Palmese group for providing TGA, Dr. Shamsabadi and Department of Chemistry for NMR measurement, and Central Research Facilities at Drexel University for providing SEM and XRD access.

References

[1] A. Manthiram, Y. Fu, S.-.H. Chung, C. Zu, Y.-.S. Su, Rechargeable lithium–sulfur batteries, Chem. Rev. 114 (2014) 11751–11787.
[2] P.G. Bruce, S.A. Freunberger, L.J. Hardwick, J.-.M. Tarascon, Li–O_2 and Li–S batteries with high energy storage, Nat. Mater. 11 (2012) 19.
[3] R. Arvidsson, M. Janssen, M. Svanström, P. Johansson, B.A. Sandén, Energy use and climate change improvements of Li/S batteries based on life cycle assessment, J. Power Sources 383 (2018) 87–92.
[4] D. Bresser, S. Passerini, B. Scrosati, Recent progress and remaining challenges in sulfur-based lithium secondary batteries–a review, Chem. Commun. 49 (2013) 10545–10562.
[5] A. Fotouhi, D. Auger, L. O'Neill, T. Cleaver, S. Walus, Lithium-sulfur battery technology readiness and applications—a review, Energies 10 (2017) 1937.
[6] Z.W. Seh, Y. Sun, Q. Zhang, Y. Cui, Designing high-energy lithium-sulfur batteries, Chem. Soc. Rev. 45 (2016) 5605–5634.
[7] D.-.W. Wang, Q. Zeng, G. Zhou, L. Yin, F. Li, H.-.M. Cheng, I.R. Gentle, G.Q.M. Lu, Carbon-sulfur composites for Li–S batteries: status and prospects, J. Mater. Chem. A 1 (2013) 9382–9394.
[8] A. Singh, V. Kalra, TiO phase stabilized into freestanding nanofibers as strong polysulfide immobilizer in Li–S batteries: evidence for Lewis acid–base interactions, ACS Appl. Mater. Interfaces 10 (2018) 37937–37947.
[9] X. Liu, J.Q. Huang, Q. Zhang, L. Mai, Nanostructured metal oxides and sulfides for lithium-sulfur batteries, Adv. Mater. 29 (2017) 1601759.
[10] L. Xiao, Y. Cao, J. Xiao, B. Schwenzer, M.H. Engelhard, L.V. Saraf, Z. Nie, G.J. Exarhos, J. Liu, A soft approach to encapsulate sulfur: polyaniline nanotubes for lithium-sulfur batteries with long cycle life, Adv. Mater. 24 (2012) 1176–1181.
[11] P.T. Dirlam, R.S. Glass, K. Char, J. Pyun, The use of polymers in Li-S batteries: a review, J. Polym. Sci. Part A. 55 (2017) 1635–1668.
[12] Y. Zhong, X. Xu, Y. Liu, W. Wang, Z. Shao, Recent progress in metal–organic frameworks for lithium-sulfur batteries, Polyhedron (2018).
[13] A. Rosenman, R. Elazari, G. Salitra, E. Markevich, D. Aurbach, A. Garsuch, The effect of interactions and reduction products of LiNO3, the anti-shuttle agent, in Li-S battery systems, J. Electrochem. Soc. 162 (2015) A470–A473.
[14] J. Scheers, S. Fantini, P. Johansson, A review of electrolytes for lithium-sulphur batteries, J. Power Sources 255 (2014) 204–218.
[15] A. Singh, A. Rafie, V. Kalra, Revisiting the use of electrolyte additives in Li-S batteries: role of porosity of sulfur host materials, Sustain. Energy Fuels (2019).
[16] R. Fang, J. Xu, D. Wang, Covalent fixing of sulfur in metal-sulfur batteries, Energy Environ. Sci. (2020).
[17] A.G. Simmonds, J.J. Griebel, J. Park, K.R. Kim, W.J. Chung, V.P. Oleshko, J. Kim, E.T. Kim, R.S. Glass, C.L. Soles, Inverse vulcanization of elemental sulfur to prepare polymeric electrode materials for Li–S batteries, ACS Macro Lett. 3 (2014) 229–232.
[18] W.J. Chung, J.J. Griebel, E.T. Kim, H. Yoon, A.G. Simmonds, H.J. Ji, P.T. Dirlam, R.S. Glass, J.J. Wie, N.A. Nguyen, The use of elemental sulfur as an alternative feedstock for polymeric materials, Nat. Chem. 5 (2013) 518.
[19] G. Hu, Z. Sun, C. Shi, R. Fang, J. Chen, P. Hou, C. Liu, H.M. Cheng, F. Li, A sulfur-rich copolymer@ CNT hybrid cathode with dual-confinement of polysulfides for high-performance lithium-sulfur batteries, Adv. Mater. 29 (2017) 1603835.
[20] Y. Zhang, J.J. Griebel, P.T. Dirlam, N.A. Nguyen, R.S. Glass, M.E. Mackay, K. Char, J. Pyun, Inverse vulcanization of elemental sulfur and styrene for polymeric cathodes in Li–S batteries, J. Polym. Sci. Part A Polym. Chem. 55 (2017) 107–116.
[21] Y. Wei, X. Li, Z. Xu, H. Sun, Y. Zheng, L. Peng, Z. Liu, C. Gao, M. Gao, Solution processible hyperbranched inverse-vulcanized polymers as new cathode materials in Li–S batteries, Polym. Chem. 6 (2015) 973–982.
[22] Q. Jiang, Y. Li, X. Zhao, P. Xiong, X. Yu, Y. Xu, L. Chen, Inverse-vulcanization of vinyl functionalized covalent organic frameworks as efficient cathode materials for Li–S batteries, J. Mater. Chem. A 6 (2018) 17977–17981.
[23] S. Shukla, A. Ghosh, P.K. Roy, S. Mitra, B. Lochab, Cardanol benzoxazines–a sustainable linker for elemental sulphur based copolymers via inverse vulcanisation, Polymer (Guildf) 99 (2016) 349–357.

[24] A. Ghosh, S. Shukla, G.S. Khosla, B. Lochab, S. Mitra, Sustainable sulfur-rich copolymer/graphene composite as lithium-sulfur battery cathode with excellent electrochemical performance, Sci. Rep. 6 (2016) 25207.
[25] C. Tran, V. Kalra, Fabrication of porous carbon nanofibers with adjustable pore sizes as electrodes for supercapacitors, J. Power Sources 235 (2013) 289–296.
[26] R. Singhal, S.-.H. Chung, A. Manthiram, V. Kalra, A free-standing carbon nanofiber interlayer for high-performance lithium-sulfur batteries, J. Mater. Chem. A 3 (2015) 4530–4538.
[27] C. Dillard, S.-.H. Chung, A. Singh, A. Manthiram, V. Kalra, Binder-free, free-standing cathodes fabricated with an ultra-rapid diffusion of sulfur into carbon nanofiber mat for lithium sulfur batteries, Materi. Today Energy 9 (2018) 336–344.
[28] N. Li, Z. Chen, W. Ren, F. Li, H.-.M. Cheng, Flexible graphene-based lithium ion batteries with ultrafast charge and discharge rates, Proc. Natl. Acad. Sci. 109 (2012) 17360–17365.
[29] J.J. Griebel, N.A. Nguyen, A.V. Astashkin, R.S. Glass, M.E. Mackay, K. Char, J. Pyun, Preparation of dynamic covalent polymers via inverse vulcanization of elemental sulfur, ACS Macro Lett. 3 (2014) 1258–1261.
[30] A. Hoefling, D.T. Nguyen, P. Partovi-Azar, D. Sebastiani, P. Theato, S.-.W. Song, Y.J. Lee, Mechanism for the stable performance of sulfur-copolymer cathode in lithium-sulfur battery studied by solid-state NMR spectroscopy, Chem. Mater. 30 (2018) 2915–2923.
[31] G. Leofanti, M. Padovan, G. Tozzola, B. Venturelli, Surface area and pore texture of catalysts, Catal. Today 41 (1998) 207–219.
[32] H.E. Gottlieb, V. Kotlyar, A. Nudelman, NMR chemical shifts of common laboratory solvents as trace impurities, J. Org. Chem. 62 (1997) 7512–7515.
[33] B.A. Trofimov, L.M. Sinegovskaya, N.K. Gusarova, Vibrations of the S–S bond in elemental sulfur and organic polysulfides: a structural guide, J. Sulfur Chem. 30 (2009) 518–554.
[34] H. He, C.-.G. Zhang, J.-.L. Xia, A.-.A. Peng, Y. Yang, H.-.C. Jiang, L. Zheng, C.-.Y. Ma, Y.-.D. Zhao, Z.-.Y. Nie, Investigation of elemental sulfur speciation transformation mediated by acidithiobacillus ferrooxidans, Curr. Microbiol. 58 (2009) 300–307.
[35] J. Coates, Interpretation of infrared spectra, a practical approach, Encyclopedia of analytical chemistry: applications, theory and instrumentation, (2006).
[36] Z. Sun, M. Xiao, S. Wang, D. Han, S. Song, G. Chen, Y. Meng, Sulfur-rich polymeric materials with semi-interpenetrating network structure as a novel lithium-sulfur cathode, J. Mater. Chem. A 2 (2014) 9280–9286.
[37] Y. Zhang, Y. Sun, L. Peng, J. Yang, H. Jia, Z. Zhang, B. Shan, J. Xie, Se as eutectic accelerator in sulfurized polyacrylonitrile for high performance all-solid-state lithium-sulfur battery, Energy Storage Mater. (2018).
[38] V.K. Shankarayya Wadi, K.K. Jena, S.Z. Khawaja, K. Yannakopoulou, M. Fardis, G. Mitrikas, M. Karagianni, G. Papavassiliou, S.M. Alhassan, NMR and EPR structural analysis and stability study of inverse vulcanized sulfur copolymers, ACS Omega 3 (2018) 3330–3339.
[39] W. Zhou, Y. Yu, H. Chen, F.J. DiSalvo, H.c.D. Abruña, Yolk-shell structure of polyaniline-coated sulfur for lithium-sulfur batteries, J. Am. Chem. Soc. 135 (2013) 16736–16743.
[40] P. McNaughter, J. Bear, A. Mayes, I. Parkin, P. O'Brien, The in situ synthesis of PbS nanocrystals from lead (II) n-octylxanthate within a 1, 3-diisopropenylbenzene–bisphenol A dimethacrylate sulfur copolymer, R. Soc. Open Sci. 4 (2017) 170383.
[41] M. Yamamoto, Y. Terauchi, A. Sakuda, M. Takahashi, Binder-free sheet-type all–solid-state batteries with enhanced rate capabilities and high energy densities, Sci. Rep. 8 (2018) 1212.
[42] B.M. Pastore, M.J. Savelski, C.S. Slater, F.A. Richetti, Life cycle assessment of N-methyl-2-pyrrolidone reduction strategies in the manufacture of resin precursors, Clean Technol. Environ. Policy 18 (2016) 2635–2647.
[43] A.-M.O. Mohamed, M. El-Gamal, Sulfur Concrete for the Construction Industry: a Sustainable Development Approach, J. Ross Publishing, 2010.
[44] S. Zeng, L. Li, L. Xie, D. Zhao, N. Wang, S. Chen, Conducting polymers crosslinked with sulfur as cathode materials for high-rate, ultralong-life lithium-sulfur batteries, ChemSusChem 10 (2017) 3378–3386.
[45] S. Shukla, A. Ghosh, U.K. Sen, P.K. Roy, S. Mitra, B. Lochab, Cardanol benzoxazine-sulfur copolymers for Li-S batteries: symbiosis of sustainability and performance, Chem. Select 1 (2016) 594–600.
[46] S. Diez, A. Hoefling, P. Theato, W. Pauer, Mechanical and electrical properties of sulfur-containing polymeric materials prepared via inverse vulcanization, Polymers (Basel) 9 (2017) 59.
[47] P.T. Dirlam, A.G. Simmonds, T.S. Kleine, N.A. Nguyen, L.E. Anderson, A.O. Klever, A. Florian, P.J. Costanzo, P. Theato, M.E. Mackay, Inverse vulcanization of elemental sulfur with 1, 4-diphenylbutadiyne for cathode materials in Li–S batteries, RSC Adv. 5 (2015) 24718–24722.
[48] X. Tao, J. Wang, C. Liu, H. Wang, H. Yao, G. Zheng, Z.W. Seh, Q. Cai, W. Li, G. Zhou, Balancing surface adsorption and diffusion of lithium-polysulfides on nonconductive oxides for lithium-sulfur battery design, Nat. Commun. 7 (2016) 11203.
[49] G. Zhou, H. Tian, Y. Jin, X. Tao, B. Liu, R. Zhang, Z.W. Seh, D. Zhuo, Y. Liu, J. Sun, Catalytic oxidation of Li2S on the surface of metal sulfides for Li− S batteries, Proc. Natl. Acad. Sci. 114 (2017) 840–845.
[50] D. Liu, C. Zhang, G. Zhou, W. Lv, G. Ling, L. Zhi, Q.H. Yang, Catalytic effects in lithium-sulfur batteries: promoted sulfur transformation and reduced shuttle effect, Adv. Sci. 5 (2018) 1700270.
[51] F. Sun, J. Wang, D. Long, W. Qiao, L. Ling, C. Lv, R. Cai, A high-rate lithium-sulfur battery assisted by nitrogen-enriched mesoporous carbons decorated with ultrafine La 2 O 3 nanoparticles, J. Mater. Chem. A 1 (2013) 13283–13289.
[52] X. Ji, S. Evers, R. Black, L.F. Nazar, Stabilizing lithium–sulphur cathodes using polysulphide reservoirs, Nat. Commun. 2 (2011) 325.
[53] S. Zeng, L. Li, J. Yu, N. Wang, S. Chen, Highly crosslinked organosulfur copolymer nanosheets with abundant mesopores as cathode materials for efficient lithium-sulfur batteries, Electrochim. Acta 263 (2018) 53–59.
[54] I. Gomez, D. Mecerreyes, J.A. Blazquez, O. Leonet, H.B. Youcef, C. Li, J.L. Gómez-Cámer, O. Bondarchuk, L. Rodriguez-Martinez, Inverse vulcanization of sulfur with divinylbenzene: stable and easy processable cathode material for lithium-sulfur batteries, J. Power Sources 329 (2016) 72–78.
[55] I. Gomez, O. Leonet, J.A. Blazquez, D. Mecerreyes, Inverse vulcanization of sulfur using natural dienes as sustainable materials for lithium-sulfur batteries, ChemSusChem 9 (2016) 3419–3425.
[56] H. Kim, J. Lee, H. Ahn, O. Kim, M.J. Park, Synthesis of three-dimensionally interconnected sulfur-rich polymers for cathode materials of high-rate lithium–sulfur batteries, Nat. Commun. 6 (2015) 7278.
[57] J. Ma, J. Fan, S. Chen, X. Yang, K.N. Hui, H. Zhang, C.W. Bielawski, J. Geng, Covalent confinement of sulfur copolymers onto graphene sheets affords ultrastable lithium-sulfur batteries with fast cathode kinetics, ACS Appl. Mater. Interfaces 11 (2019) 13234–13243.
[58] J. Key, Y. Feng, J. Shen, P. Wang, H. Wang, H. Liang, R. Wang, S. Ji, A highly crosslinked and conductive sulfur-rich copolymer with grafted polyaniline for stable cycling lithium-sulfur batteries, J. Electrochem. Soc. 167 (2020) 020530.
[59] Y. Zhao, Y. Zhang, Z. Bakenova, Z. Bakenov, Carbon/sulfur composite cathodes for flexible lithium/sulfur batteries: status and prospects, Front. Energy Res. 3 (2015) 2.
[60] A. Singh, V. Kalra, Electrospun nanostructures for conversion type cathode (S, Se) based lithium and sodium batteries, J. Mater. Chem. A 7 (2019) 11613–11650.